Applied Radiation and Isotopes 224 (2025) 111923

Contents lists available at ScienceDirect

Applied Radiation and Isotopes

journal homepage: www.elsevier.com/locate/apradiso

Impact of diorites and feldspars on soil radioactivity: Evidence from university city of the Universidad Nacional Mayor de San Marcos and the National Institute of Neoplastic Diseases

E.G. Villarreyes Peña [a,b,*], G. Patiño Camargo [a,b], P. Mendoza [d], O. Baltuano Elias [a,b,c]

[a] Faculty of Physical Sciences, Universidad Nacional Mayor de San Marcos, Lima 15081, Peru
[b] Biophysics and Medical Physics Laboratory, Research Group on Physical Instrumentation and Applications (INFISA), Faculty of Physical Sciences, Universidad Nacional Mayor de San Marcos, Lima 15081, Peru
[c] Electronic Development Laboratory, Research and Development Directorate, Peruvian Institute of Nuclear Energy (IPEN), Av. Canadá 1480, Lima, 41, Peru
[d] Division of Nuclear Analytical Techniques, Peruvian Institute of Nuclear Energy (IPEN), Lima, Peru

ARTICLE INFO

Keywords:
Natural radiation
HPGe semiconductors
NORM
Gamma spectroscopy
Absorbed dose
Dose equivalent
Hazards index

ABSTRACT

This study represents the first systematic measurement of environmental radiation in the University City of the Universidad Nacional Mayor de San Marcos (UNMSM) and the National Institute of Neoplastic Diseases (INEN) in the city of Lima, Peru, conducted between July, December 2022, and January 2023. Natural radioactivity levels and absorbed dose rates in soil samples were determined by using gamma spectroscopy with a high purity germanium detector (HPGe) semiconductor detector with 150 % efficiency.

At UNMSM, the following results were obtained for the activity concentrations (A) of the four main naturally occurring radioactive materials NORM (^{238}U, ^{226}Ra, ^{232}Th, and ^{40}K): $A_{U238} = 24.2 \pm 3.4\ Bq\ kg^{-1}$, $A_{Ra226} = 28.8 \pm 0.7\ Bq\ kg^{-1}$, $A_{Th232} = 39.4 \pm 1.2\ Bq\ kg^{-1}$ and $A_{K40} = 539 \pm 7\ Bq\ kg^{-1}$. We find the absorbed dose rate of 57.5 $nGy\ h^{-1}$ and an annual effective dose equivalent of 0.28 $mSv\ y^{-1}$. On the other hand, at INEN, the following activity concentrations of NORM were found: $A_{U238} = 26.0 \pm 3.4\ Bq\ kg^{-1}$, $A_{Ra226} = 27.9 \pm 0.8\ Bq\ kg^{-1}$, $A_{Th232} = 42.1 \pm 1.6\ Bq\ kg^{-1}$ and $A_{K40} = 559 \pm 7.8\ Bq\ kg^{-1}$. We found the annual absorbed dose rate of 60.7 $nGy\ h^{-1}$ and an annual effective dose equivalent of 0.30 $mSv\ y^{-1}$. Additionally, the equivalent activity in radium (Req) and the risk indices for both indoor and outdoor environments were also determined.

The higher than global average values of ^{40}K activity concentrations are due to the greater presence of diorites and feldspars in the alluvial soils of Lima. These findings highlight the geological influence on local environmental radioactivity and are essential for future risk assessments. Nonetheless, the levels of environmental radioactivity found in this study are safe for the population in urban areas of academic and medical importance.

1. Introduction

Natural radiation is a phenomenon present in our environment and that comes from natural sources, such as soil, water, food, construction materials, also from artificial sources, and cosmic radiation. Exposure to this radiation can have effects on human health depending on the dose rate, so it is important to understand its distribution and radiation levels in different locations. In this sense, there are several techniques and tools to analyze natural radiation in soils and obtain detailed information about the radionuclides that are present. In the specific case of the capital of Peru, the study of natural radiation in the soils of the National University of San Marcos (UNMSM) and the National Institute of Neoplastic Diseases (INEN) has gained increasing relevance, given that the city of Lima has a high population density, which elevates the potential exposure of large segments of the population to natural sources of radiation. UNMSM is one of the country's leading academic and scientific research institutions, while INEN is the most important hospital center specialized in cancer treatment; the latter must ensure that environmental radiation levels do not adversely affect patients undergoing medical therapy.

Since the Oscar Miroquesada de la Guerra Nuclear Power Plant (RACSO) came into operation in 1988 in the district of Carbayllo, Lima-Peru, no radiological map of the city of Lima has been produced. Environmental radioactivity measurements have only been carried out in the

* Corresponding author. Faculty of Physical Sciences, Universidad Nacional Mayor de San Marcos (UNMSM), Av. Amézaga 375, Lima, 1, Peru.
E-mail address: eduardo.villarreyes@unmsm.edu.pe (E.G. Villarreyes Peña).

https://doi.org/10.1016/j.apradiso.2025.111923
Received 24 February 2025; Received in revised form 15 May 2025; Accepted 19 May 2025
Available online 24 May 2025

area of influence up to 1.0 km from the nuclear reactor (Osores, 2021).

Assessing ionizing radiation in both an educational and a hospital setting not only enables the establishment of an environmental baseline for radiological monitoring purposes, but also contributes to ensuring the radiological safety of staff, students, patients, and visitors. To measure environmental radioactivity from the main naturally occurring radioactive materials (NORM) in soils at both UNMSM and INEN, a non-destructive gamma-ray spectroscopy technique has been employed. (UNSCEAR, 1982; UNSCEAR, 2000; Gilmore, 2008; Knoll, 2010; IAEA, 2019; Vajda et al., 2020).

2. Materials and methods

2.1. Sample collection and preparation

Since 1966, what would be called University City (U.C) de UNMSM, located in the district of Lima Cercado (12°03′24.7"S; 77°04′58.4"W), came into operation; this consists of approximately 676 004 m^2, of which to date are parks, sidewalks, roads and squares. Other parts have intangible archaeological sites, vegetated areas and uncultivated land.

On the other hand, the INEN since 1988 is working in the district of Surquillo (12°06′42.4"S; 76°59′54.6"W); It has about 47 986 m^2 and is made up of buildings, patios, sidewalks, tracks and green areas.

The sampling points, both at the University City of UNMSM and the National Institute of Neoplastic Diseases (INEN), correspond to geological units of the Q1Sc type (Quaternary-Pleistocene, ancient alluvial deposits). These units are characterized by their sedimentary origin, consisting primarily of materials transported and deposited by ancient fluvial processes. The sediments originate from the erosion of the Andes, where diverse rock types, including igneous and sedimentary varieties, contribute to the composition of these soils.

Various geological studies (Palacios et al., 1992; INGEMMET, 2023) have confirmed that these soils contain notable amounts of diorites and feldspars, which are key contributors to the observed levels of natural radioactivity. Diorites, as intrusive igneous rocks, are rich in minerals such as plagioclase feldspars and biotite, both of which may contain trace amounts of potassium (K) and uranium (U). Feldspars, particularly potassium feldspar, are significant sources of ^{40}K, a naturally occurring radionuclide that contributes to gamma radiation in the environment.

A stratified systematic random sampling statistical methodology was applied for sample collection, taking into account the Q1Sc geological units (Quaternary–Pleistocene, ancient alluvial deposits) identified by INGEMMET as predominant in both sites (UNMSM and INEN). Six random points per stratum were selected using a random number generator, ensuring spatial representativeness and accuracy in the measurement of natural radioactivity and absorbed dose rates (Beretka and Mathew, 1985; Arnedo et al., 2017; IAEA, 2019).

A grid was established on both campuses (Fig. 1), stratified according to the typical geomorphological characteristics of the Q1Sc deposits (slope <5 %, loamy sand texture), within which the sampling points were selected following the protocols of ISO Standard 18589-7 (2021) for studies of soil radioactivity. Samples were collected at a depth not

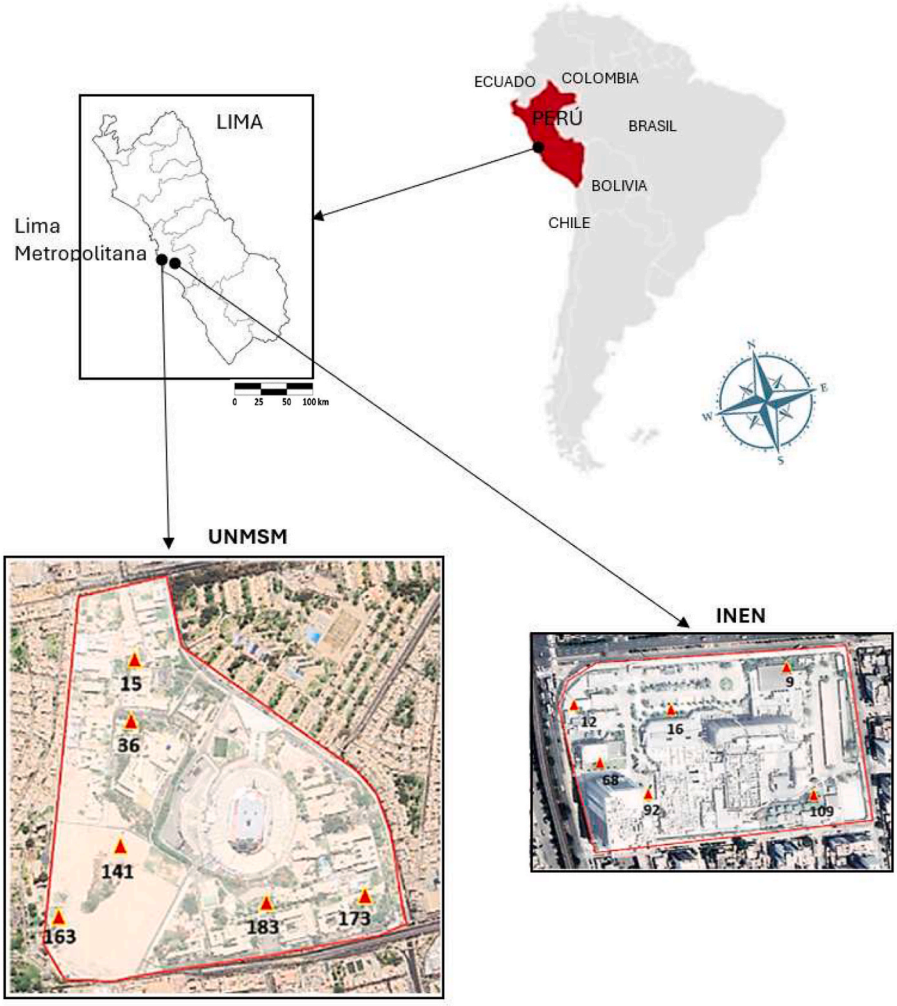

Fig. 1. Geographical location of the sample points for UNMSM and INEN. Map data© 2018 google.

exceeding 10.0 cm (corresponding to the characteristic surface horizon of these deposits), with a standard volume of 500 g per point. The sample size (n = 6 per site) was determined through statistical power analysis (β = 0.8, α = 0.05), taking into account the area of the grounds (0.68 km^2 for UNMSM and 0.05 km^2 for INEN) and the lithological homogeneity of the Q1Sc units reported by INGEMMET in previous studies on alluvial soils in Lima. Geological homogeneity was confirmed using Kruskal-Wallis tests among quadrants ($p > 0.05$), validating the methodological approach in accordance with environmental radiological surveillance standards (Arnedo et al., 2017; ISO-18589-3, 2018).

Soil samples were collected between July, September and December 2021 and January 2022. They were then packed in plastic bags and labeled by the sampling point. The samples were then taken to the Biophysics and Medical Physics Laboratory of the Physical Instrumentation and Applications research group (INFISA) attached to the UNMSM Research Vice-Rectorate for preparation. This first consisted of removing large stones and plant remains, then sieving at 500 μm, recording its wet weight and finally going through a drying process in a muffle for 24 h at about 105 ± 5 °C. Subsequently, the samples were transferred to Petri-type containers of 95 ± 2 mm in diameter and 15 ± 1 mm in height, with an average mass of 95 ± 2 g per sample, to then seal them and leave them for 30 days to establish secular equilibrium to then seal them and leave them for 30 days in order to establish secular equilibrium between ^{226}Ra and its short-lived gamma-emitting progeny. (CSN, 2003; Romero et al., 2010; IAEA, 2019).

Finally, the samples were taken to the IPEN (Peruvian Nuclear Energy Institute) in Hurangal, where they were put into a 150 % efficient high purity germanium detector (HPGe) to determine their gamma activity.

2.2. Instrumentation and calibration

In the Neutron Activation Analysis laboratory, within the Nuclear and Analytical Techniques Division of IPEN, at the RACSO nuclear reactor facilities in Hurangal, Lima-Peru, there is a HPGe coaxial semiconductor detector, brand CAMBERRA model GC15022, of 150 % relative efficiency with respect to NaI, whose resolution is 2.2 keV at 1.33 Mev and 1.3 keV at 122 keV, in addition to a peak/Compton ratio of 80:1, with a detector diameter of 90.80 mm (3.6 in) and height of 90.00 mm (3.5 in). The entire detector is connected to a model 2002CSL-10 preamplifier, model 2026 amplifier, a model 3125 high-voltage source and a model 7500 S L cryostat, all from CAMBERRA.

The detector is housed in a CAMBERRA model 767 lead armor system, has a lead thickness of 100 mm (3.9 in) and is encased in an outer steel casing of 9.5 mm (0.4 in). The coating consists of a 1 mm (0.04 in) thick layer of tin and a 1.5 mm (0.06 in) thick layer of copper. Interior dimensions are 280 mm (11.0 in) diameter by 406 mm (16.0 in) high (Fig. 2).

For the set-up of the HPGe detector, 4096 channels were used, then an energy calibration using a ^{152}Eu source whose geometry is a disk of 25.1 ± 0.5 mm in diameter and with an activity of 355.7 ± 7 kBq (01/01/1981).

The energy-dependent efficiency calibration was performed using an Eckert & Ziegler No. 2277-15 multinuclide standard solution (10.39109 g, 373.7 kBq, reference date January 11, 2021), covering an energy range of 60 keV–1800 keV to ensure proper detector characterization.

The process involved mixing the standard solution with a soil matrix of similar composition to the analyzed samples, ensuring equivalent geometric conditions (Petri-type container of known dimensions). The sample was then homogenized in a mixing device for 3 h and sealed to prevent volatilization losses.

Measurements were conducted using a CANBERRA GC15022 HPGe detector, with the sample positioned 100 mm from the detector window to minimize true coincidence summing effects. Corrections for this effect were applied using EFFTRAN v4.72 software, which implements efficiency transfer through numerical calculations based on: physical

Fig. 2. Chain for gamma spectroscopy with the HPGe detector of 150 % efficiency, together with the shield, its Dewar and electronic chain in the Division of Analytical and Nuclear Techniques of IPEN.

detector models, source-detector geometry, sample dimensions and radionuclide decay schemes (including energy levels, emission intensities, half-lives, and gamma-gamma coincidences).

The efficiency curve was fitted using a polynomial/logarithmic regression model, yielding a correlation coefficient ($R^2 = 0.99$), Where equation (1). Calibrations are verified semiannually (last performed on September 12, 2023, per laboratory protocol) using certified reference materials to ensure metrological traceability. (Moens et al., 1981; Daza et al., 2001; Vidmar et al., 2011; Jonsson et al., 2015) (Table 1 Fig. 3).

$$\begin{gathered} \varepsilon\,(E) = 0.002{*}E - 0.1095, 60.0 \;< E \;< 92.8\;keV \\ \varepsilon\,(E) = -0.046{*}Ln(E) + 0.3876, 92.8 \;< E <\; 1800.0\;keV \\ R^2 = 0.99 \end{gathered} \tag{1}$$

2.3. Activity concentrations determination

The soil samples were placed in the gamma spectrometry chain for a time of 86 400 s. The gamma spectra of the different samples were analyzed with the commercial software Genie2000.

The radioactive activity concentrations A(Bq kg^{-1}) was determined from the equation:

$$A = \frac{N}{I\,\varepsilon\,m\,t_v\,f} \tag{2}$$

Where N: net photopeak counts, I: emission probability intensity at a certain energy, ε: efficiency at a certain energy, t_v: corrected time and f: is the correction factor, where self-absorption, decay, random sum and sum by coincidences were considered. To ensure accuracy in the determination of specific activities of radionuclides present in environmental soil samples, a true coincidence summing (TCS) correction was applied during the efficiency calibration phase of the gamma

Table 1
Efficiency values after a regression adjustment.

E	ε	Δε
63.3	0.0197	0.0038
92.8	0.0800	0.0037
238.6	0.1358	0.0033
351.9	0.1179	0.0030
609.3	0.0926	0.0024
911.2	0.0741	0.0016
969.0	0.0713	0.0015
1001.0	0.0698	0.0014
1460.8	0.0524	0.0002
1764.5	0.0437	0.0006

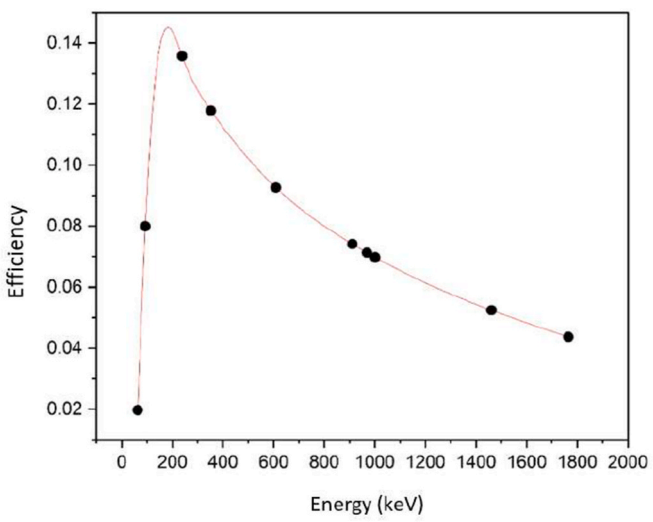

Fig. 3. Efficiency curve for energies used in this study.

spectrometric system. This correction was performed using the EFFTRAN program, taking into account the actual measurement geometry (Petri-type container placed over a Canberra HPGe coaxial detector, model GC15022). The model incorporated the main gamma lines of cascade-emitting radionuclides such as ^{214}Bi and ^{228}Ac, associated with the ^{226}Ra and ^{232} Th day series, respectively. The corrected efficiency was subsequently used for the quantification of ^{235}U, ^{226}Ra, ^{232}Th, and ^{40}K, with results compared against the certified reference material IAEA-312. Relative deviations remained below 10 %, ensuring the validity of the applied method. For the identification of the main NORM such as ^{238}U, the photopeaks of ^{234}Th (63.03 keV) and ^{234m}Pa (1000.85 keV) were analyzed; for ^{226}Ra, the photopeaks of ^{214}Pb (351.91 keV), ^{214}Bi (609.26 keV and 1764.36 keV) were analyzed; for ^{232}Th, the ^{212}Pb (238.57 keV), ^{228}Ac (911.11 keV and 968.98 keV) photopeaks were analyzed and for ^{40}K, the 1460.80 keV photopeak was analyzed (Fig. 4). In interpreting the activity concentrations of the radionuclide ^{232}Th, we initially assumed secular equilibrium with its decay products ^{228}Ra and ^{228}Th (a conventional approach for well) sealed soil samples. However, to validate this assumption, we experimentally compared measured activities of ^{228}Ra and ^{228}Th through 1) Sequential measurements over 3 months, 2) Activity ratio analysis, and 3) Exclusion of chemically altered samples. Results confirm equilibrium within 5 % (k = 2) for 97 % of processed samples, which constitute the dataset presented in this study. (ISO.18589-7, 2018).

2.4. Dose calculation

The evaluation of the radiological risk associated with the exposure of radionuclides in the soil, if a uniform distribution is considered, at 1 m from the soil surface, is measured by the Absorbed Dose Rate (D) or gamma dose rate in the air. For this we resort to equation (3) that relates the activities of ^{226}Ra, ^{232}Th and ^{40}K in Bq kg^{-1} (UNSCEAR, 1982; Sohrabi, 1998; Rani and Singh, 2005; ICRP, 2007; Taskin et al., 2009; Alkhomashi, et al., 2011; Ribeiro et al., 2018; Castillo Corzo et al., 2025).

$$D = 0.462\,A_{Ra} + 0.604A_{Th} + 0.0417\,A_K \quad (3)$$

Where A_{Ra}: activity concentrations of ^{226}Ra, A_{Th} activity concentrations of ^{232}Th, A_K: activity concentrations of ^{40}K and D: $nGy\,h^{-1}$.

2.5. Effective annual equivalent dose

It is a measure used in radiation protection to assess the amount of

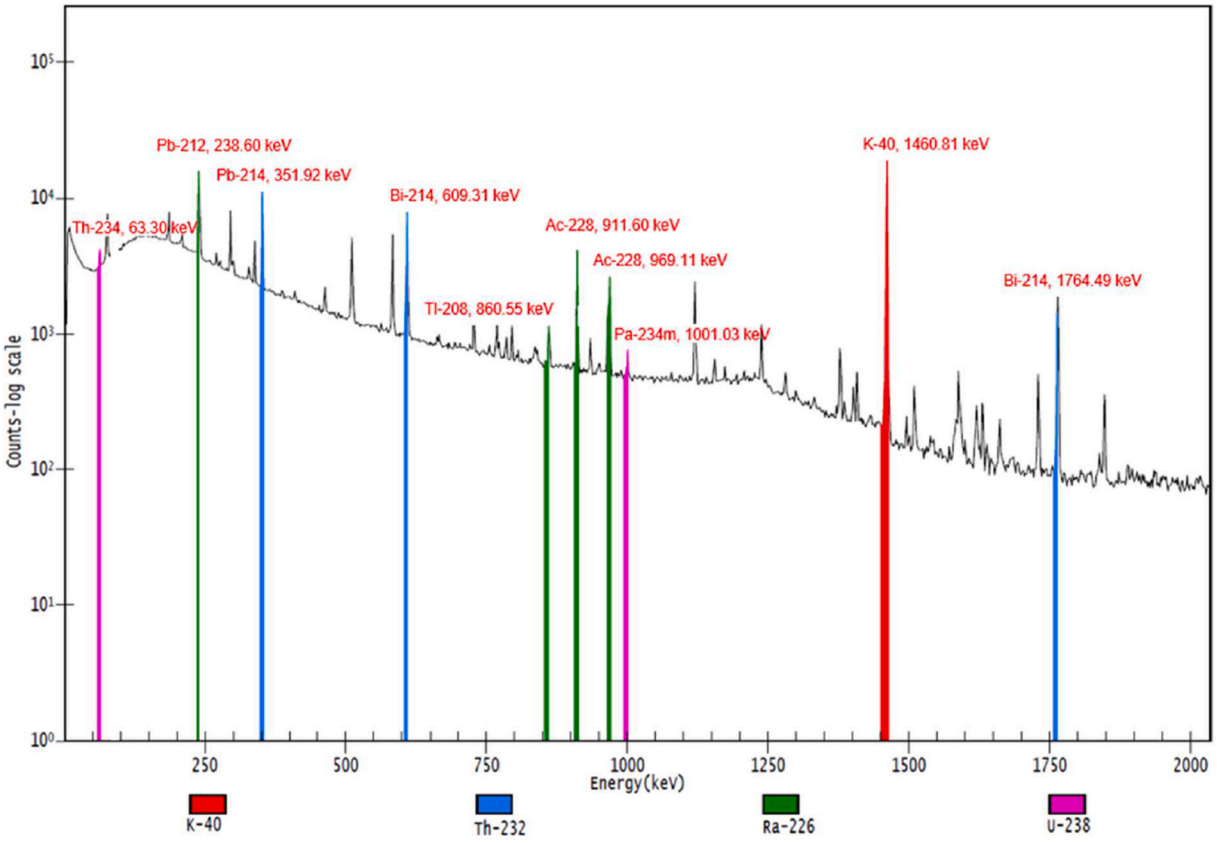

Fig. 4. Gamma spectrum acquired from a sample in a HPGe detector, where the photopeaks can be seen for the analysis of the main radionuclides.

radiation absorbed by an individual in a period of one year. It is widely used in environmental radiation studies to assess the potential risk of radiation exposure and establish safe dose limits. It is estimated using the following equations for indoor $AEDE_i$ and outdoor $AEDE_O$ (UNSCEAR, 1982; Ribeiro et al., 2018):

$$AEDE_O = D \times 8760 \times 0.2 \times 0.7 \times 10^{-6} \quad (4)$$

$$AEDE_i = D \times 8760 \times 0.8 \times 0.7 \times 10^{-6} \quad (5)$$

Where $AEDE_O$ and $AEDE_i$: $mSv\,y^{-1}$

2.6. Radio equivalent activity

This parameter is used to characterize the content of ^{226}Ra, ^{232}Th and ^{40}K in a radioactive material. The concept is based on the fact that the radiation emitted by radium, thorium and potassium can have a biological effect similar to that of a specific amount of the children of radium and radon. It is determined using the equation (UNSCEAR, 1982; Beretka and Mathew, 1985)

$$Ra_{eq} = A_{Ra} + 1.43\,A_{Th} + 0.077\,A_K \quad (6)$$

Where A_{Ra}: activity concentrations of ^{226}Ra, A_{Th} activity concentrations of ^{232}Th, A_K: activity concentrations of ^{40}K and Ra_{eq} : $Bq\,kg^{-1}$

2.7. Risk index

If we assume that the maximum allowed value of the radio equivalent is 370 Bq kg^{-1}, the risk assessment index (H) is defined when it is assumed that the effective annual dose from construction materials is 1 mSv y^{-1}, thus we have the equations (UNSCEAR, 1982; Beretka and Mathew, 1985; Xinwei, 2005; Alkhomashi, et al., 2011):

$$H_{ext} = \frac{A_{Ra}}{370} + \frac{A_{Th}}{259} + \frac{A_K}{4810} \leq 1 \quad (7)$$

$$H_{int} = \frac{A_{Ra}}{185} + \frac{A_{Th}}{259} + \frac{A_K}{4810} \leq 1 \quad (8)$$

where A_{Ra}: activity concentrations of ^{226}Ra, A_{Th} activity concentrations of ^{232}Th y A_K: activity concentrations of ^{40}K.

3. Results and discussion

The values of the activity concentrations of the different soil samples in the U.C of the UNMSM using equation (2), are shown in Table 2 where it can be seen that the average activity concentrations of ^{238}U is 24.2 ± 3.4 Bq kg^{-1}, which is below the world average which is 33 Bq kg^{-1} (UNSCEAR, 2008). The average activity concentrations of ^{226}Ra is 28.8 ± 0.7 Bq kg^{-1}, which is lower than the world average of 32 Bqkg^{-1} (UNSCEAR, 2008). The average activity concentrations of ^{232}Th is 39.4 ± 1.2 Bq kg^{-1}, which is below the world average of 45 Bq kg^{-1} (UNSCEAR, 2008). The average activity concentrations of ^{40}K is 539.3 ± 7.3 Bq kg^{-1}, which is 1.28 above the world average of 420 Bq kg^{-1}, but within the range of 140–850 Bq kg^{-1} (UNSCEAR, 2008).

The activity concentrations values of the different INEN soil samples using equation (2) are shown in Table 2 where the average activity concentrations of ^{238}U is 26.0 ± 3.4 Bq kg^{-1}, which is below the world average which is 33 Bq kg^{-1} (UNSCEAR, 2008). The average activity concentrations of ^{226}Ra is 27.9 ± 0.8 Bq kg^{-1}, which is lower than the world average of 32 Bq kg^{-1} (UNSCEAR, 2008). The average activity concentrations of ^{232}Th is 42.1 ± 1.6 Bq kg^{-1}, which is below the world average of 45 Bq kg^{-1} (UNSCEAR, 2008). The average activity concentrations of ^{40}K is 559.4 ± 7.8 Bq kg^{-1}, which is 1.33 above the world average of 420 Bq kg^{-1}, but within the range of 140–850 Bq kg^{-1} (UNSCEAR, 2008).

When examining the case of ^{40}K, it is known that natural potassium is primarily composed of three isotopes: ^{39}K (93.26 %), ^{40}K (0.0117 %), and ^{41}K (6.73 %) (Garner et al., 1975). Although ^{40}K is the least abundant, its significance lies in its radioactivity. This property makes ^{40}K an important source of natural radioactivity. In his study on the relationship between U and Th in granitic rocks, Whitfield found that radioactivity in igneous rocks is closely related to their primary mineralogy (Whitfield, 1959; Faure and Mensing, 2005). In the absence of direct mineralogical analyses such as XRD or ICP-OES, geochemical ratios K/Th, K/U, and U/Th were employed as indirect inference tools to determine the predominant lithological type, as shown in Table 3. These ratios fall within the typical ranges for granitic rocks (K/Th = 10–15; K/U = 10–30) and for diorites containing potassium feldspars, which often exhibit similar values due to relative depletion in uranium and thorium and enrichment in potassium (Clark et al., 1966; Chiozzi et al., 2002; Faure and Mensing, 2005). In our case, the measured activity of

Table 3
Geochemical ratios K/Th, K/U, and U/Th based on mean values from the UNMSM and INEN sites.

	K/Th	K/U	U/Th
UNMSM	13.7	22.3	0.6
INEN	13.3	21.5	0.6

Table 2
Radioactive activity concentrations in Bq kg^{-1} of the different samples.

Sample	Position		Activity (Bq kg^{-1})			
			U-238	Ra-226	Th-232	K-40
UNMSM-15	12°03′10.9"S	77°05′11.5"W	22.1 ± 3.4	30.6 ± 0.8	43.1 ± 1.4	585.7 ± 8.1
UNMSM-36	12°03′16.6"S	77°05′12.0"W	24.8 ± 3.7	30.0 ± 0.8	38.9 ± 1.3	532.1 ± 7.4
UNMSM-141	12°03′27.7"S	77°05′10.9"W	24.7 ± 3.6	27.3 ± 0.7	36 ± 1.2	529.9 ± 7.2
UNMSM-163	12°03′35.1"S	77°05′19.4"W	24.0 ± 3.2	23.7 ± 0.6	34.5 ± 1	465.2 ± 6.1
UNMSM-173	12°03′34.1"S	77°04′57.8"W	24.0 ± 3.1	28.0 ± 0.7	36.3 ± 1.1	516.6 ± 6.8
UNMSM-183	12°03′33.3"S	77°04′49.8"W	25.6 ± 3.6	33.1 ± 0.9	47.7 ± 1.5	606.5 ± 8.2
		Mean	24.2 ± 3.4	28.8 ± 0.7	39.4 ± 1.2	539.3 ± 7.3
		Range	22.1–25.6	23.7–33.1	34.5–47.7	465.2–606.5
INEN-9	12°06′43.3"S	76°59′52.0"W	23.3 ± 3.5	28.6 ± 0.8	47.0 ± 1.5	594.5 ± 8.1
INEN-12	12°06′44.1"S	76°59′59.3"W	27.0 ± 3.9	28.3 ± 0.8	44.1 ± 1.4	597.5 ± 8.1
INEN-16	12°06′43.4"S	76°59′55.8"W	25.6 ± 3.8	28.7 ± 0.8	48.0 ± 1.5	590.4 ± 8
INEN-68	12°06′45.9"S	76°59′58.3"W	24.3 ± 3.4	27.2 ± 0.7	42.4 ± 1.4	560.6 ± 7.6
INEN-92	12°06′46.7"S	76°59′56.8"W	25.3 ± 3.4	26.8 ± 0.7	38.1 ± 1.2	517.6 ± 7
INEN-109	12°06′46.6"S	76°59′51.1"W	24.3 ± 3.4	26.7 ± 0.7	36.4 ± 1.2	508.3 ± 7
		Mean	25.0 ± 3.6	27.7 ± 0.8	42.7 ± 1.4	561.5 ± 7.6
		Range	23.3–27.0	26.7–28.7	36.4–48.0	508.3–597.5
		World reference	33	32	45	420
		World range	16–110	17–60	11–64	140–850

^{40}K in dioritic soils correlates with feldspathic rocks such as granites and diorites; the presence of potassium-rich minerals (orthoclase, microcline, and biotite) explains the detected ^{40}K concentrations. The average activity of 539.3 Bq·kg^{-1} recorded in our samples corresponds to a K_2O content of approximately 1.5–2.5 %, which is consistent with moderately potassic diorites.

Therefore, this indirect evidence suggests that the elevated ^{40}K content at both sites is linked to felsic lithology with significant contributions of potassium feldspars derived from the weathering of diorites from the Coastal Batholith, a well-documented geological formation underlying Metropolitan Lima (Palacios et al., 1992; Rollinson, 1993; Winter, 2014).

These values are in agreement with those found in the study on soil activity concentrations in the city of Pernambuco, Brazil, conducted by (Do Carmo Leal et al., 2020) where an activity of 20 Bq kg^{-1} for ^{226}Ra and 458 Bq kg^{-1} for ^{40}K was reported. They also relate to the study on undisturbed soils in the northeast of Buenos Aires province, Argentina, carried out by (Montes et al., 2012) which reported activities of 27.8 Bq kg^{-1} for ^{226}Ra, 33.3 Bq kg^{-1} for ^{232}Th, and 614 Bq kg^{-1} for ^{40}K. Our data are consistent with the findings of (Reino et al., 2018) who reported activity concentrations in soils near the Tungurahua volcano in Ecuador of 27.58 ± 1.99 Bq kg^{-1} for ^{226}Ra, 30.28 ± 2.48 Bq kg^{-1} for ^{232}Th, and 411 ± 28.77 Bq kg^{-1} for ^{40}K.

The average absorbed dose rates are shown in Table 4, using equation (3) in the U.C of UNMSM the average is 57.5 nGy h^{-1}, which is 1.13 higher than the world average of 51 nGy h^{-1} (UNSCEAR, 2000). The average annual indoor dose equivalent using equation (4) is 0.28 mSv y^{-1} which is less than the world average which is 0.41 mSv y^{-1} and the average annual outdoor dose equivalent using equation (5) is of 0.07 mSv y^{-1} which is equal to the world average (UNSCEAR, 2000).

From the samples in INEN, the average absorbed dose rate found is 60.7 nGy h^{-1}, which is 1.19 higher than the world average of 51 nGy h^{-1} (UNSCEAR, 2000). The annual equivalent dose indoors on average is 0.30 mSv y^{-1}, which is a lower value than the world average, which is 0.41 mSv y^{-1}, and the annual equivalent dose outdoors on average is 0.07 mSv y^{-1}, which coincides with the world average (UNSCEAR, 2000).

From Table 5, the equivalent in radius is shown, using equation (6), thus we have that in the University City of the UNMSM an average value of 126.7 Bq kg^{-1} is obtained. For the external risk index using equation (7), an average of 0.34 was determined and for the average internal risk index using equation (8), an average of 0.42 is obtained.

Table 4
Absorbed dose rate and internal and external annual equivalent dose of the different samples.

Sample	D (nGy h^{-1})	AEDEi (mSv y^{-1})	AEDEo (mSv y^{-1})
UNMSM-15	60.7	0.30	0.07
UNMSM-36	57.1	0.28	0.07
UNMSM-141	55.3	0.27	0.07
UNMSM-163	51.3	0.25	0.06
UNMSM-173	54.6	0.27	0.07
UNMSM-183	65.9	0.32	0.08
Mean	57.5	0.28	0.07
Range	51.3–65.9	0.25–0.32	0.06–0.08
INEN-9	63.9	0.31	0.08
INEN-12	64.1	0.31	0.08
INEN-16	65.4	0.32	0.08
INEN-68	60.4	0.30	0.07
INEN-92	56.3	0.28	0.07
INEN-109	54.4	0.27	0.07
Mean	60.7	0.30	0.07
Range	54.4–65.4	0.27–0.32	0.07–0.08
World reference	51	0.41	0.07

Table 5
Equivalent in radius and external and internal risk index of the different samples.

Sample	Raeq (Bq kg^{-1})	Hext	Hint
UNMSM-15	137.4	0.37	0.45
UNMSM-36	126.5	0.34	0.42
UNMSM-141	119.6	0.32	0.40
UNMSM-163	108.9	0.29	0.36
UNMSM-173	119.7	0.32	0.40
UNMSM-183	147.9	0.40	0.49
Mean	126.7	0.34	0.42
Range	108.9–147.9	0.29–0.40	0.36–0.49
INEN-9	141.5	0.38	0.45
INEN-12	137.4	0.37	0.42
INEN-16	142.8	0.39	0.40
INEN-68	126.4	0.34	0.36
INEN-92	121.1	0.33	0.40
INEN-109	117.9	0.32	0.49
Mean	131.2	0.35	0.42
Range	117.9–141.5	0.32–0.39	0.36–0.49

4. Conclusions

The present study has determined the values of radioactive activity in the superficial soils of the main NORM at UNMSM and INEN; showing us results that are below the world average (^{226}Ra, ^{238}U and ^{232}Th) and above the world average (^{40}K), compared to the UNSCEAR, 2008 data. In addition, we have found the absorbed dose rate is within the world ranges and the effective annual dose equivalent whose mean is below the world values; according to the data compared with the UNSCEAR, 2000 report. We have also determined the equivalent radium activity whose average for UNMSM is 126.7 Bq kg^{-1} and for INEN 131.2 Bq kg^{-1}. The external and internal risk index for UNMSM is 0.34 and 0.42; for the INEN it is 0.35 and 0.42 respectively.

The alluvial soils at the sampling sites in Lima, formed by the erosion and deposition of material originating from the Andes, exhibit a significant concentration of minerals such as feldspars and fragments of dioritic rocks. The positive correlation between K_2O content (1.5–2.5 %) and ^{40}K activity reinforces the role of local lithology as a primary control on natural radioactivity. This potassium-rich mineralogical composition explains the relatively high levels of ^{40}K activity observed. These findings suggest that in future studies (using techniques such as XRD, ICP-OES), the spatial distribution of ^{40}K could be used as a tracer of geodynamic processes in alluvial environments, with observed variations reflecting differences in the composition of the source units exposed in the Andes.

Overall, the levels of environmental radioactivity found are safe for students, professors, workers, patients, and the public. This study can serve as a reference to establish a future radiological baseline in the soils of Lima, providing crucial data to assess and manage radioactivity risks in urban areas.

CRediT authorship contribution statement

E.G. Villarreyes Peña: Writing – review & editing, Writing – original draft, Software, Methodology, Investigation, Data curation, Conceptualization. **G. Patiño Camargo:** Writing – original draft, Methodology, Investigation. **P. Mendoza:** Data curation. **O. Baltuano Elias:** Writing – original draft, Supervision, Software, Funding acquisition, Formal analysis, Data curation.

Declaration of competing interest

The authors declare that they have no known competing financial interests or personal relationships that could have appeared to influence the work reported in this paper.

Acknowledgments

We thank Mg. Daniela Alexandra León Castillo for the translation of this manuscript. To the students Jerson Rivas, Luis Angulo, Senayda

Ortiz, Antonella Anticona, Lucero Cisneros, Ayrton Nalvarte, César Morales and Jhann Reyes for your collaboration in this project. Also, to the Vice-rectorate of research the UNMSM for providing the facilities in achieving the project.

Data availability

Data will be made available on request.

References

Alkhomashi, N., Al-Dahan, N., 2011. Determination of the natural radioactivity in Qatarian building materials using high-resolution gamma-ray spectrometry. Nuclear Instruments and Methods in Physics Research A 652, 915–919.

Arnedo, M.A., Rubiano, J.G., Alonso, H., Tejera, A., et al., 2017. Mapping natural radioactivity of soils in the eastern Canary Islands. J. Environ. Radioact. 166, 242–258.

Castillo Corzo, M., Peña Rodríguez, V., Manrique Nugent, M., Villarreyes Peña, E., Byrne, P., González Gonzalez, J.C., De Los Santos Valladares, L., 2025. Potentially toxic elements and radionuclides contamination in soils from the vicinity of an ancient mercury mine in Huancavelica, Peru. Soil Science Annual 76 (2), 204389.

Chiozzi, P., Pasquale, V., Verdoya, M., 2002. Naturally occurringradioactivity at the Alps–Apennines transition. Radiat. Meas. 35, 147–154.

Clark, S.P., Peterman, Z.E., Heier, K.S., 1966. SECTION 24: ABUNDANCES of URANIUM, THORIUM, and POTASSIUM. Handbook of Physical Constants, pp. 521–542.

CSN, 2003. Procedimiento para la conservación y preparación de muestras de suelo para la determinación de la radiactividad. Colección Informes Técnicos 11.

Daza, M.J., Quintana, B., Garcia Tavalera, M., Fernandez, F., 2001. Efficiency calibration of a HPGe detector in the 46.54-2000 keV energy range for the measurement of environmental samples. Nucl. Instrum. Methods Phys. Res., Sect. A 470 (N° 3), 520–532.

Do Carmo Leal, A.L., Da Costa Lauria, D., Ca Riberiro, F., Paim Viglio, E., 2020. Spatial distributions of natural radionuclides in soils of the state of Pernambuco, Brazil: influence of bedrocks, soils types and climates. J. Environ. Radioact. 211 (1), 106046.

Faure, G., Mensing, T.M., 2005. Isotopes: Principles and Applications, third ed. Wiley.

Beretka, J., Mathew, P.J., 1985. Natural radioactivity of Australian building materials, industrial wastes and by-products. Health Phys. 48 (1), 87–95. https://doi.org/10.1097/00004032-198501000-00007. PMID: 3967976.

Garner, E.L., Murphy, T.J., Gramlich, J.W., Paulsen, P.J., Barnes, I.L., 1975. Absolute Isotopic Abundance Ratios and the Atomic Weight of a Reference Sample of Potassium. J Res Natl Bur Stand A Phys Chem 79A (6), 713–725. https://doi.org/10.6028/jres.079A.028. PMID: 32184525; PMCID: PMC6589417.

Gilmore, G., 2008. Practical Gamma-Ray Spectrometry. John Wiley & Sons, Ltd, pp. 131–140.

IAEA, 2019. Guidelines on Soil and Vegetation Sampling for Radiological Monitoring, Technical Reports Series No. 486. International Atomic Energy Agency, Vienna.

ICRP, 2007. The 2007 recommendations of the international commission on radiological protection. ICRP Publication 103 Ann. ICRP 37, 2–4.

INGEMMET, 2023. Mapa geológico del Perú. https://portal.ingemmet.gob.pe/web/guest/mapa-geologico-nacional. (Accessed 2 January 2023).

ISO.18589-3, 2018. Measurement of Radioactivity in the Environment - Soil - Part 3: Test Method of Gamma-Emitting Radionuclides Using Gamma-Ray Spectrometry.

ISO.18589-7, 2018. Measurement of Radioactivity in the Environment - Soil - Part 7: in Situ Measurement of Gamma-Emitting Radionuclides.

Jonsson, S., Vidmar, T., Ramebäck, H., 2015. Implementation of calculation codes in gamma spectrometry measurements for corrections of systematic effects. J. Radioanal. Nucl. Chem. 303, 1727–1736. https://doi.org/10.1007/s10967-014-3748-z.

Knoll, G., 2010. Radiation Detection and Measurement, fourth ed. J. Wiley and Sons, New York, p. 830.

Moens, L., De Donder, J., Lin, X., et al., 1981. Calculation of the absolute peak efficiency of gamma-ray detectors for different counting geometries. Nucl. Instrum. Methods 187, 451–472.

Montes, M.L., Mercader, R.C., Taylor, M.A., Runco, J., 2012. Assessment of natural radioactivity levels and their relationship with soil characteristics in undisturbed soils of the northeast of Buenos Aires province, Argentina. J. Environ. Radioact. 105 (2), 30–39.

Osores, L., 2021. Línea Base Radiológica Ambiental en el Centro Nuclear RACSO (1980-2020). Revista ECIPerú. https://revistaeciperu.com/wp-content/uploads/2022/01/reciperu202145Osores.pdf. (Accessed 8 January 2023).

Palacios, O., Caldas, J., Vela, Ch, 1992. Geología de los cuadrángulos de Lima, Lurín, Chancay y Chosica. Hojas 25-i, 25-j. 24-i, 24-j INGEMMET, Boletín, Serie A: Carta Geológica Nacional, vol. 43, p. 163. https://hdl.handle.net/20.500.12544/163. (Accessed 28 January 2023).

Rani, A., Singh, S., 2005. Natural radioactivity levels in soil samples from some areas of Himachal Pradesh, India using γ-ray spectrometry. Atmos. Environ. 39 (34), 6306–6314.

Reino, W., Pucha, G., Recalde, C., 2018. Occurrence of radioactive materials in pyroclastic flows of Tungurahua volcano using gamma spectrometry. AIP Conference Proceedings, 2018, 020014. https://pubs.aip.org/aip/acp/article/2003/1/020014/731428/Occurrence-of-radioactive-materials-in-pyroclastic. Accessed date: 8 January 2023.

Ribeiro, F.C.A., Silva, J.I.R., Lima, E.S.A., et al., 2018. Natural radioactivity in soils of the state of rio de janeiro (Brazil): radiological characterization and relationships to geological formation, soil type sand soil properties. J. Environ. Radioact. 182, 34–43.

Rollinson, H.R., 1993. Using Geochemical Data: Evaluation, Presentation, Interpretation. Longman Scientific & Technical.

Romero, M.L., Barrera, M., y, F. Valiño., 2010. Evaluación de la Intercomparación CSN/CIEMAT-2008 entre Laboratorios Nacionales de Radiactividad Ambiental (Fosfoyeso). In: Informes Técnicos CIEMAT, n.º, 1204. CIEMAT, Madrid.

Sohrabi, M., 1998. State-of-the-Art on worldwide studies in some environments with elevated natural occurring radioactive material. Appl. Radiat. Isot. 49 (3), 169–188.

Taskin, H., Karavus, M., Topuzoghi, P. Ay, Hindiroglu, S., Karaha, G., 2009. Radionuclide concentrations in soil and lifetime cancer risk due to the gamma radioactivity in Kirklareli. J. Environ. Radioact. 100, 49–53.

UNSCEAR, 1982. Ionizing Radiation, Sources and Biological Effect United Nations Scientific Committee on the Effect of Atomic Radiation (New York).

UNSCEAR, 2000. Ionizing Radiation, Sources and Biological Effect United Nations Scientific Committee on the Effect of Atomic Radiation (New York).

UNSCEAR, 2008. Ionizing Radiation, Sources and Biological Effect United Nations Scientific Committee on the Effect of Atomic Radiation (New York).

Vajda, N., Pöllänen, R., Martin, P., Kim, Ch, 2020. Handbook of Radioactivity Analysis Volume 1: Radiation Physics and Detectors. Academic Press is an imprint of Elsevier, pp. 505–510.

Vidmar, T., Kanisch, G., Vidmar, G., 2011. Calculation of true coincidence summing corrections for extended sources with EFFTRAN. Appl. Radiat. Isot. 69, 908–911.

Whitfield, G., 1959. Uranium and thorium content of granitic rocks and their radioactivity. Geochem. Cosmochim. Acta 17 (1–2), 49–62. https://doi.org/10.1016/0016-7037(59)90038-1.

Winter, J.D., 2014. Principles of Igneous and Metamorphic Petrology, second ed. Pearson.

Xinwei, L., 2005. Natural radioactivity in some building materials of Xi'an, China. Radiat. Meas. 40 (1), 94–97.